Supplemental Material

Lingyu Meng,[1] Yiteng Jin,[2] Yichao Guan,[3] Jiayi Xu,[4] and Jie Lin[1,2]

[1] *Peking-Tsinghua Center for Life Sciences, Academy for Advanced Interdisciplinary Studies, Peking University, Beijing 100871, China*

[2] *Center for Quantitative Biology, Academy for Advanced Interdisciplinary Studies, Peking University, Beijing 100871, China*

[3] *Department of Physics, University of Illinois Urbana-Champaign, Urbana, IL 61801, USA*

[4] *Yuanpei College, Peking University, Beijing 100871, China*

(Dated: July 11, 2023)

A. Effects of the active random force on the friction coefficient

Generally, the active random force can generate an additional friction coefficient $\zeta_i = Aa_i^\gamma / k_B T_{\rm act}$, which is proportional to the magnitude of the active force and inversely proportional to an active temperature $T_{\rm act}$ [1–3]. The equation of motion becomes

$$(\eta_i + \zeta_i)\frac{\mathrm{d}r_{i,\alpha}}{\mathrm{d}t} = -\frac{\partial U}{\partial r_{i,\alpha}} + \xi_{i,\alpha} + \kappa_{i,\alpha}. \tag{1}$$

The active friction coefficient can be negligible if the active temperature $T_{\rm act}$ is much higher than the thermal temperature T. Biologically, the active random force comes from the collision of small background molecules, e.g., amino acids and ions. The active temperature satisfies $k_B T_{\rm act} = v^2 \tau \eta$, where v is the velocity of the small background particle, τ is the relaxation time of the velocity's autocorrelation function, and η is the friction coefficient of the small particle [1, 4]. For a passive system with $T_{\rm act} = T$, the relaxation time $\tau = m/\eta$ where m is the amino acid mass. We take $m = 110$ Da and $a = 0.5$ nm, and use the Stokes formula with water viscosity to compute η for an average amino acid molecule [5], and find $\tau \approx 1.94 \times 10^{-14}$ s. On the other hand, the velocity can be estimated from the equipartition theorem $v = \sqrt{k_B T/m} = 1.50 \times 10^2$ m/s. Therefore, the characteristic ballistic length in a passive system $l = v\tau = 2.91 \times 10^{-3}$ nm, which is extremely small.

Due to the numerous active processes in living cells, active molecules are expected to have longer ballistic lengths, so the active temperature should be higher than the thermal temperature [1, 2, 6]. Assuming a ballistic length around 0.5 nm, still much smaller than protein sizes, we estimate the active temperature to be $T_{\rm act} = 172T$, much higher than the thermal temperature. We confirm theoretically that the active friction coefficient is negligible given such a high ratio in the dilute limit (Figure S14a). We also simulate Eq. (1) directly with $T_{\rm act} = 100T$. The simulation results match the experimental data, the same as the model without the active friction coefficient (Figure S14b), further supporting the validity of our model. Therefore, we think that the effect of this active friction coefficient should be negligible when analyzing the diffusion enhancement.

[1] A. Solon and J. M. Horowitz, On the einstein relation between mobility and diffusion coefficient in an active bath, Journal of Physics A: Mathematical and Theoretical **55**, 184002 (2022).

[2] A. Shakerpoor, E. Flenner, and G. Szamel, The einstein effective temperature can predict the tagged active particle density, The Journal of Chemical Physics **154**, 184901 (2021).

[3] O. Granek, Y. Kafri, and J. Tailleur, Anomalous transport of tracers in active baths, Physical Review Letters **129**, 038001 (2022).

[4] A. P. Solon, Y. Fily, A. Baskaran, M. E. Cates, Y. Kafri, M. Kardar, and J. Tailleur, Pressure is not a state function for generic active fluids, Nature Physics **11**, 673 (2015).

[5] R. Milo and R. Phillips, *Cell biology by the numbers* (Garland Science, 2015).

[6] F. S. Gnesotto, F. Mura, J. Gladrow, and C. P. Broedersz, Broken detailed balance and non-equilibrium dynamics in living systems: a review, Reports on Progress in Physics **81**, 066601 (2018).

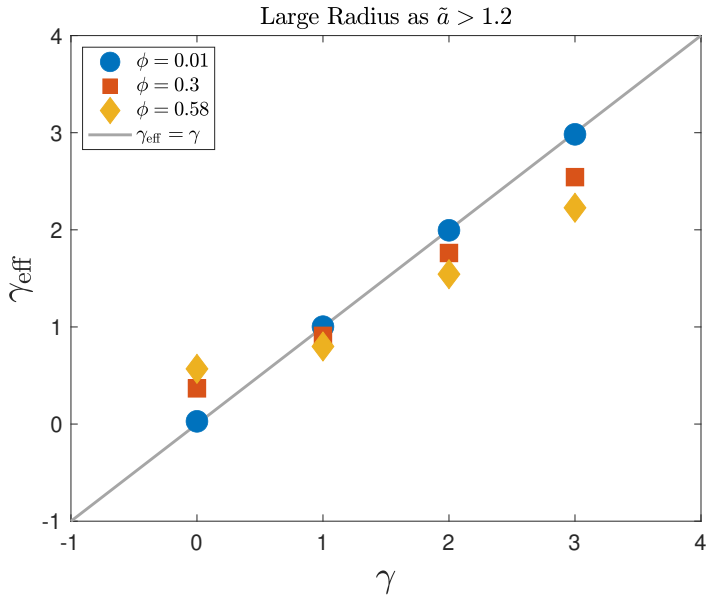

FIG. S1. The effective exponent γ_{eff} *vs.* γ for large particles with $\tilde{a} > 1.2$. The exponent γ_{eff} is equal to γ in the dilute limit. Under high volume fractions, $\gamma_{\text{eff}} > \gamma$ for $\gamma < 1$ and $\gamma_{\text{eff}} < \gamma$ for $\gamma > 1$. Here, $N = 1000$.

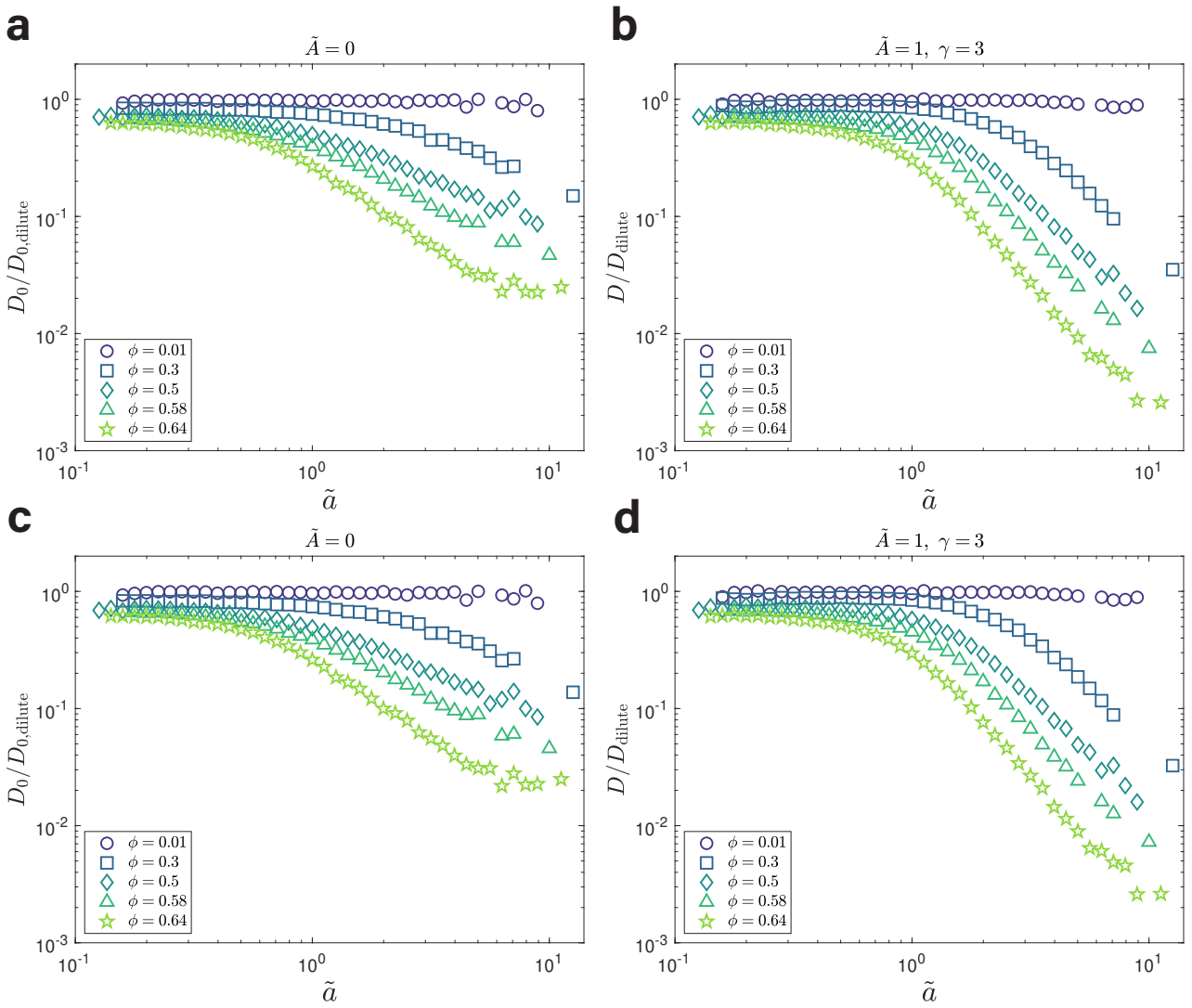

FIG. S2. Diffusion constants of the simulated polydisperse systems with different methods. (a) The ratios of the diffusion constants of a passive system relative to the dilute limit using a larger $\Delta\tilde{t}$. $\Delta\tilde{t}$ is the time interval to compute the diffusion constant, as $D = \langle \Delta\tilde{\mathbf{r}}^2(\Delta\tilde{t})\rangle/6\Delta\tilde{t}$. $\tilde{a}$ is the dimensionless radius. (b) The same analysis as (a) but for an active system. (c) A similar analysis as (a) with the diffusion constants obtained by fitting the MSDs as $\langle \Delta\tilde{\mathbf{r}}^2\rangle = 6D\Delta\tilde{t}$ between $\Delta\tilde{t}/10$ and $\Delta\tilde{t}$. The results are very close to (a). (d) The same analysis as (c) but for an active system. In all panels, $\Delta\tilde{t}$ is the time where the mean square displacement $\langle \Delta\tilde{\mathbf{r}}^2(\Delta\tilde{t})\rangle = \tilde{L}^2/32$ so that the finite system size does not affect the results. The results are binned over particles with a bin interval of 0.05 in the $\log_{10}$ scale. For the active systems, $\tilde{A} = 1$ and $\gamma = 3$. In all panels, $N = 1000$.

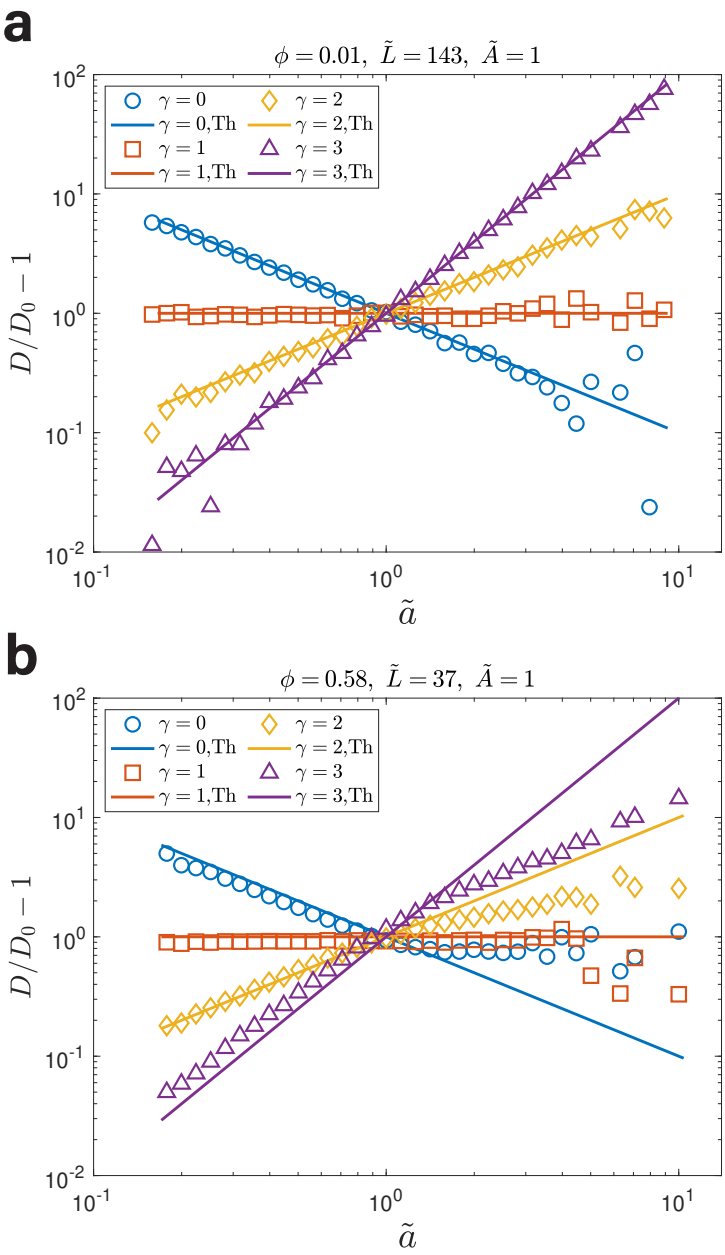

FIG. S3. The relative enhancement of the diffusion constants $D/D_0 - 1$ using a larger $\Delta\tilde{t}$ (see Figure S2). (a) $\phi = 0.01$ and (b) $\phi = 0.58$. The results are binned over particles with a bin interval of 0.05 in the $\log_{10}$ scale. The solid lines are the theoretical prediction in the dilute limit. For the active systems, $\tilde{A} = 1$. In both panels, $N = 1000$.

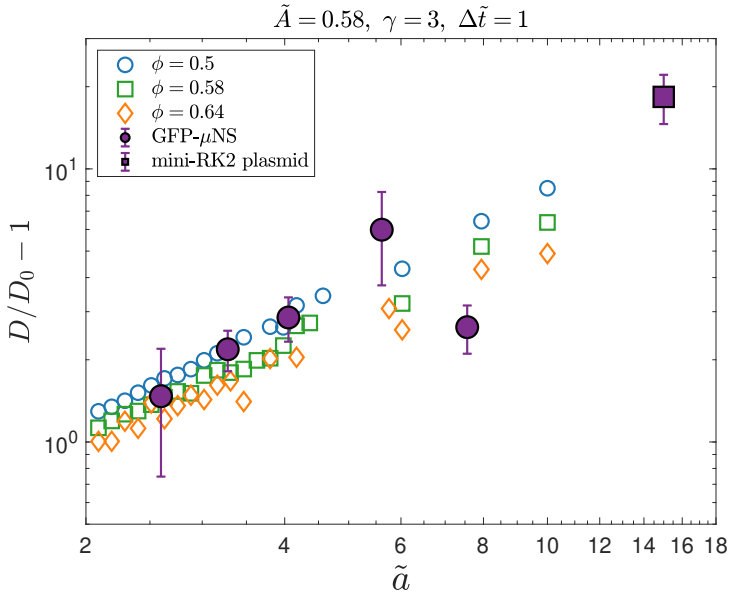

FIG. S4. Comparison between simulations and experiments using the lognormal distribution with $\sigma = 0.5$. Three particles with radii equal to 6, 8 and 10 are added to the system to mimic the experimental condition and cover a more extensive range of radius. The relative enhancements of diffusion constants from the experimental data match the simulation results reasonably well. Here, $\tilde{A} = 0.58$ and $\gamma = 3$. The results are binned over particles with a bin interval of 0.02 in the $\log_{10}$ scale. In this figure, $N = 4000$.

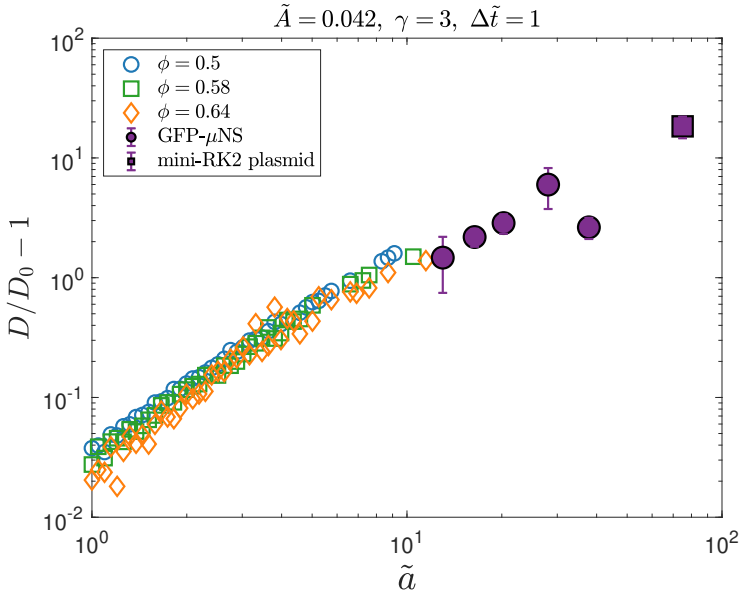

FIG. S5. Comparison between simulations and experiments with $a_0 = 2$ nm. The relative enhancements of diffusion constants $(D/D_0 - 1)$ from the experimental data match the simulation results reasonably well. Here, $\tilde{A} = 0.042$ and $\gamma = 3$. The results are binned over particles with a bin interval of 0.02 in the $\log_{10}$ scale. In this figure, $N = 1000$.

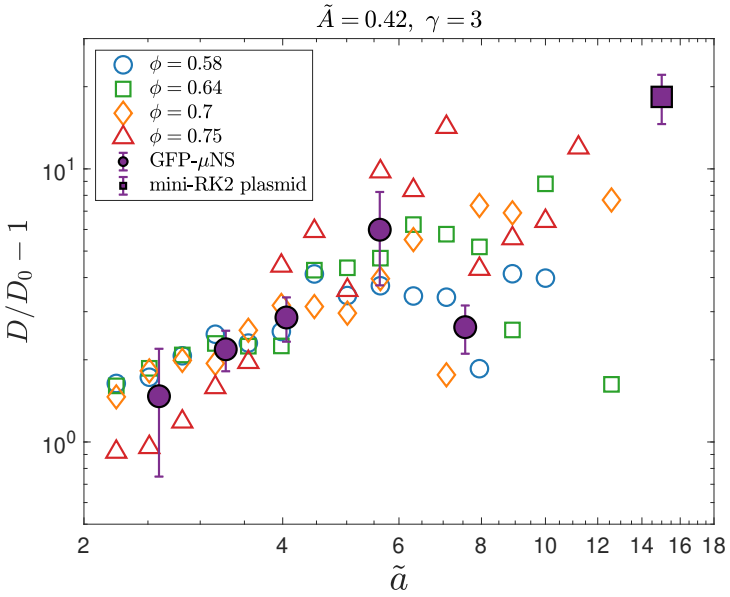

FIG. S6. The same analysis as Figure 4a in the main text, using a larger $\Delta\tilde{t}$ to compute the diffusion constant (see Figure S2). The results are binned over particles with a bin interval of 0.05 in the $\log_{10}$ scale.

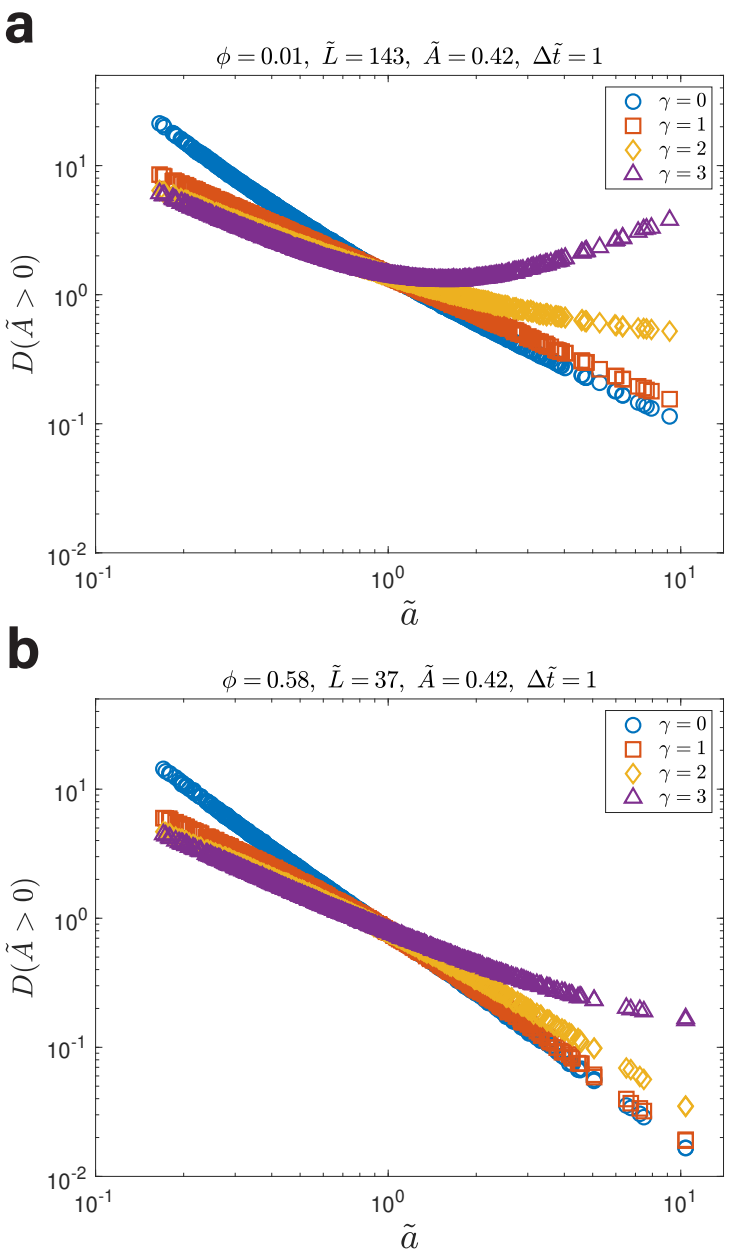

FIG. S7. The diffusion constants of active systems. (a) $\phi = 0.01$ and (b) $\phi = 0.58$. In the dilute limit, an active random force with $\gamma = 3$ leads to a non-monotonic diffusion constant as a function of the particle radius. However, in systems with a high volume fraction, the diffusion constant decreases with the particle radius. In both panels, $\tilde{A} = 0.42$ and the time interval to compute the diffusion constants is $\Delta\tilde{t} = 1$. In both panels, $N = 1000$.

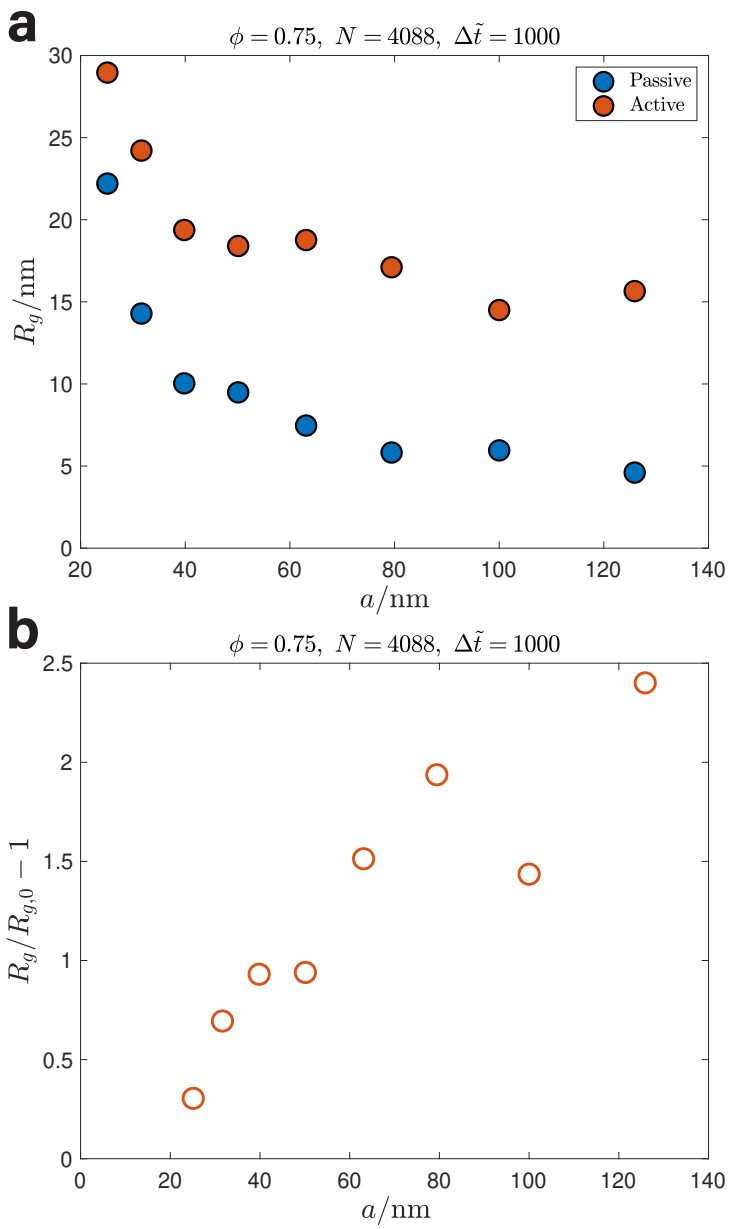

FIG. S8. Radii of gyration (R_g) for both passive and active systems with $\phi = 0.75$. (a) Radii of gyration of large particles for both passive ($R_{g,0}$) and active systems (R_g) within a dimensionless time 1000. The radii of gyration decrease linearly with the particle radius in both systems approximately. (b) The ratio of the radii of gyration between active and passive particles as $R_g/R_{g,0} - 1$ increases linearly with the particle radius approximately, similar to experimental results. In both panels, the radius is converted to physical length using $a_0 = 10$ nm. The data are binned with a window of 0.1 in the logarithmic space of radius. For the active system, $\tilde{A} = 0.42$ and $\gamma = 3$. In both panels, $N = 4000$.

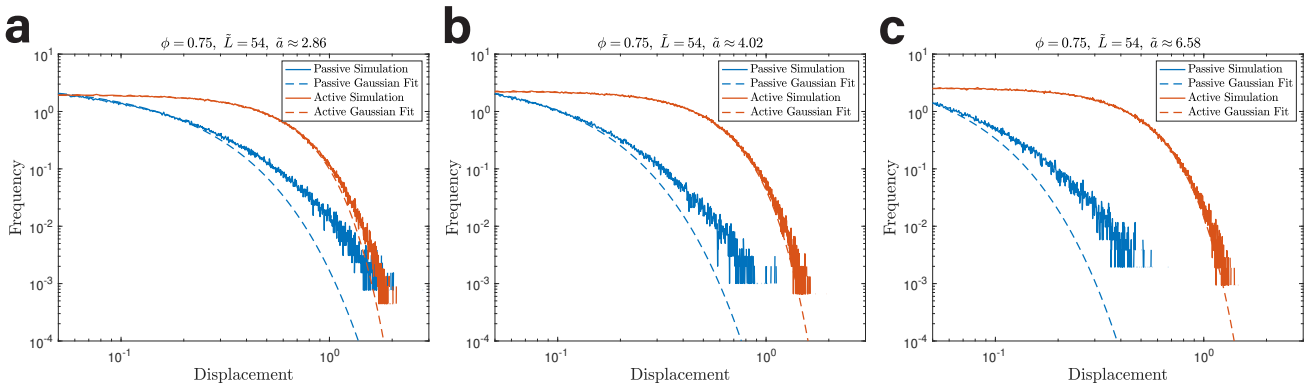

FIG. S9. Displacement distributions for passive and active systems with different particle radii. (a) The displacement distribution in the passive system has a long tail compared with the Gaussian fit, which is the dashed line. However, the distribution in the active system is closer to the Gaussian fit. The displacement distributions are calculated over 50 particles with similar radii within a time interval $\Delta\tilde{t} = 1$. The average radius over these particles is $\tilde{a} \approx 2.86$. (b) The same analysis as (a) but for $\tilde{a} \approx 4.02$. (c) The same analysis as (a) but for $\tilde{a} \approx 6.58$. For the active systems, $\tilde{A} = 0.42$ and $\gamma = 3$. In all panels, $\phi = 0.75$ and $N = 4000$.

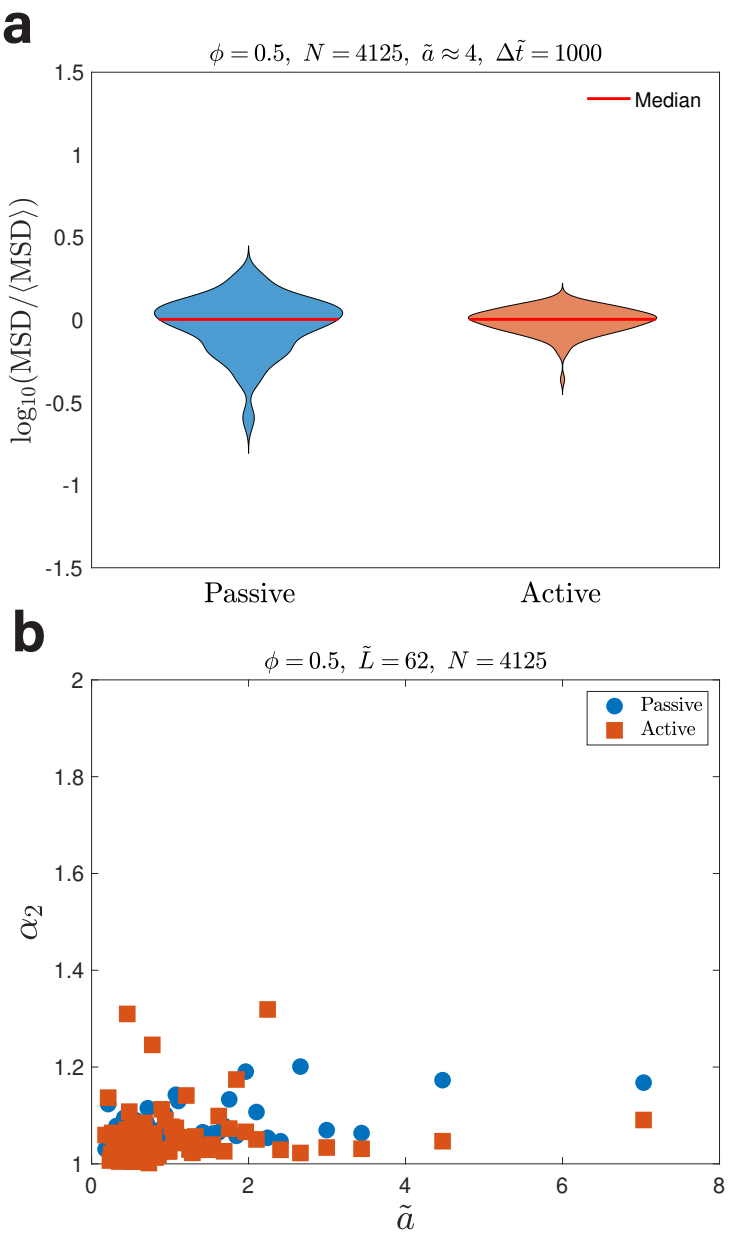

FIG. S10. Glassy-like properties are not obvious under low volume fraction. (a) With $\phi = 0.5$, the distributions of MSDs for both passive and active particles whose $\tilde{a} \approx 4$ become narrower, which means weaker dynamical heterogeneity. The MSDs within a dimensionless time 1000 are shown in the log scale and normalized by the average value. (b) With $\phi = 0.5$, α_2 of both passive and active particles are close to 1, which indicates nearly Gaussian motions. The results are averaged with 50 particles in each bin. For the active systems, $\tilde{A} = 0.42$ and $\gamma = 3$. In both panels, $N = 4000$.

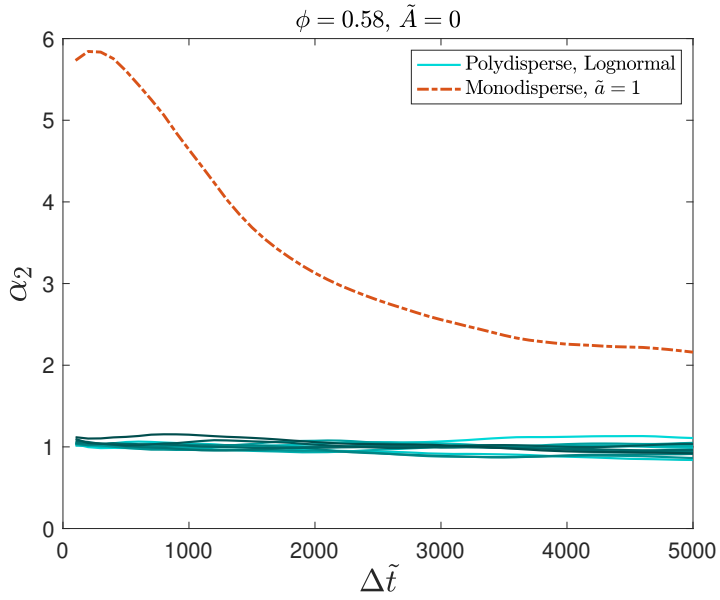

FIG. S11. The non-Gaussian parameter α_2 for polydisperse and monodisperse systems. $\Delta\tilde{t}$ is the duration of the displacement. The green lines are particles with different radii from the polydisperse simulations. All green lines are close to 1, which indicates Gaussian distribution. The orange line is obtained from the monodisperse system, indicating non-Gaussian displacement distributions. In both systems, $\phi = 0.58$ and $\tilde{A} = 0$. The α_2 are calculated with displacements without the periodic boundary condition. In both systems, $N = 1000$.

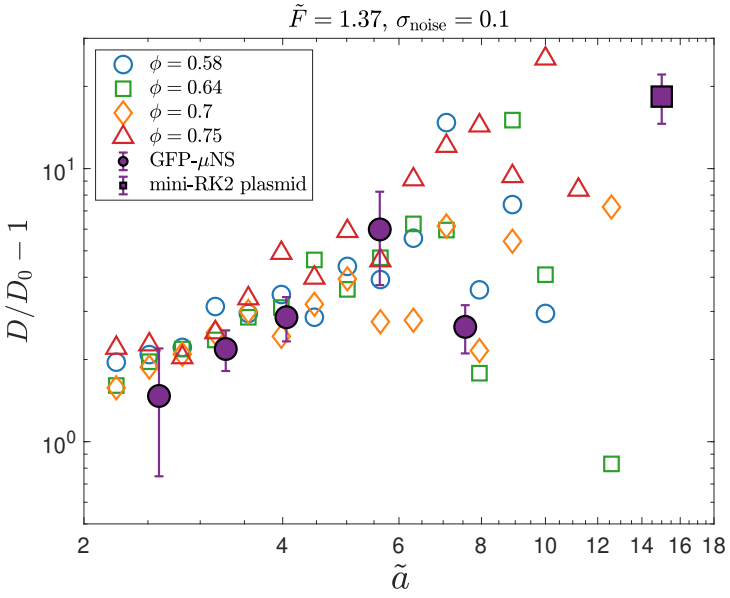

FIG. S12. The same analysis as Figure 4b in the main text, but the force obeys a size-independent normal distribution: $\tilde{F} = \tilde{F}_0[1 + \mathcal{N}(0, \sigma_{\text{noise}})]$, where $\mathcal{N}(0, \sigma_{\text{noise}})$ is a normal random number with zero average and standard deviation, σ_{noise}. The results are binned over particles with a bin interval of 0.05 in the $\log_{10}$ scale. Here, $\tilde{F}_0 = 1.38$, $\sigma_{\text{noise}} = 0.1$, and $N = 4000$.

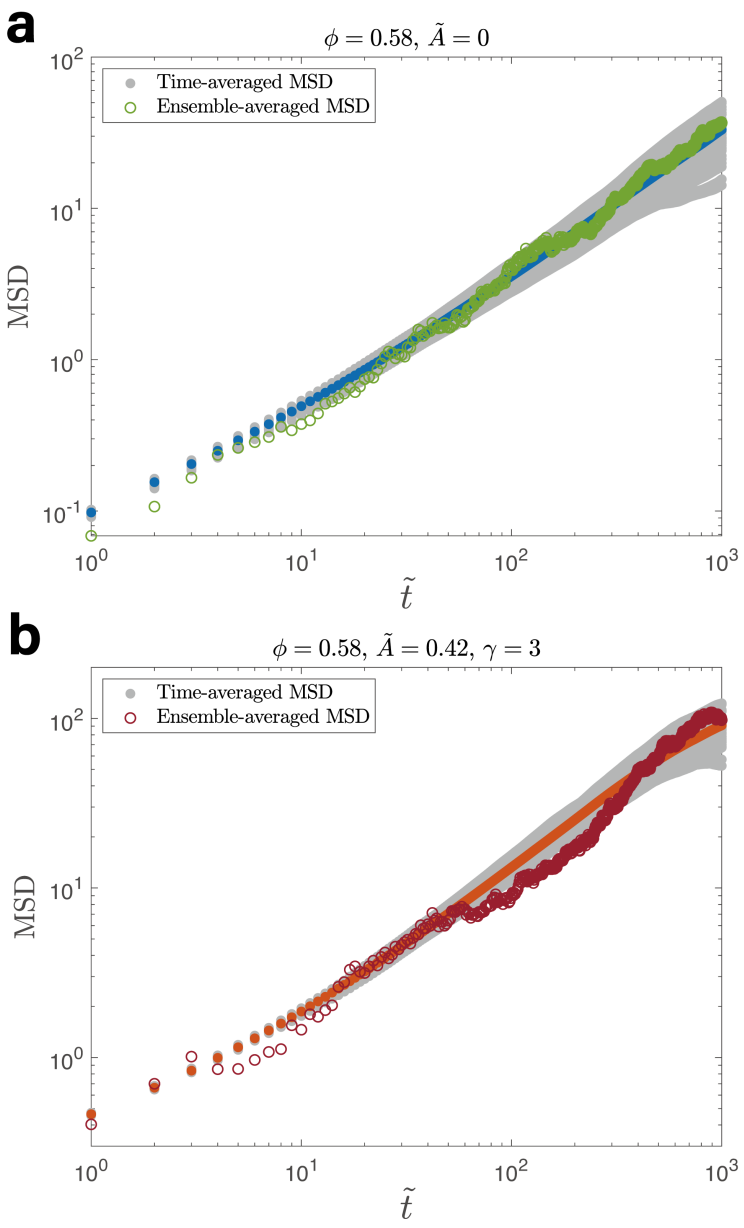

FIG. S13. Comparison between ensemble-averaged MSDs and time-averaged MSDs. (a) Analysis of passive systems. Ensemble-averaged MSDs are averaged over 100 independent simulations (corresponding to distinct cells in experiments). Time-averaged MSDs are averaged over time using one simulation with total duration $\tilde{t} = 10^4$. The blue circles are the averaged time-averaged MSD over independent simulations. (b) The same analysis of active systems where the orange circles are the averaged time-averaged MSD over independent simulations. In (a) and (b), $\phi = 0.58$. For the active system, $\tilde{A} = 0.42$ and $\gamma = 3$. In both panels, $N = 1000$.

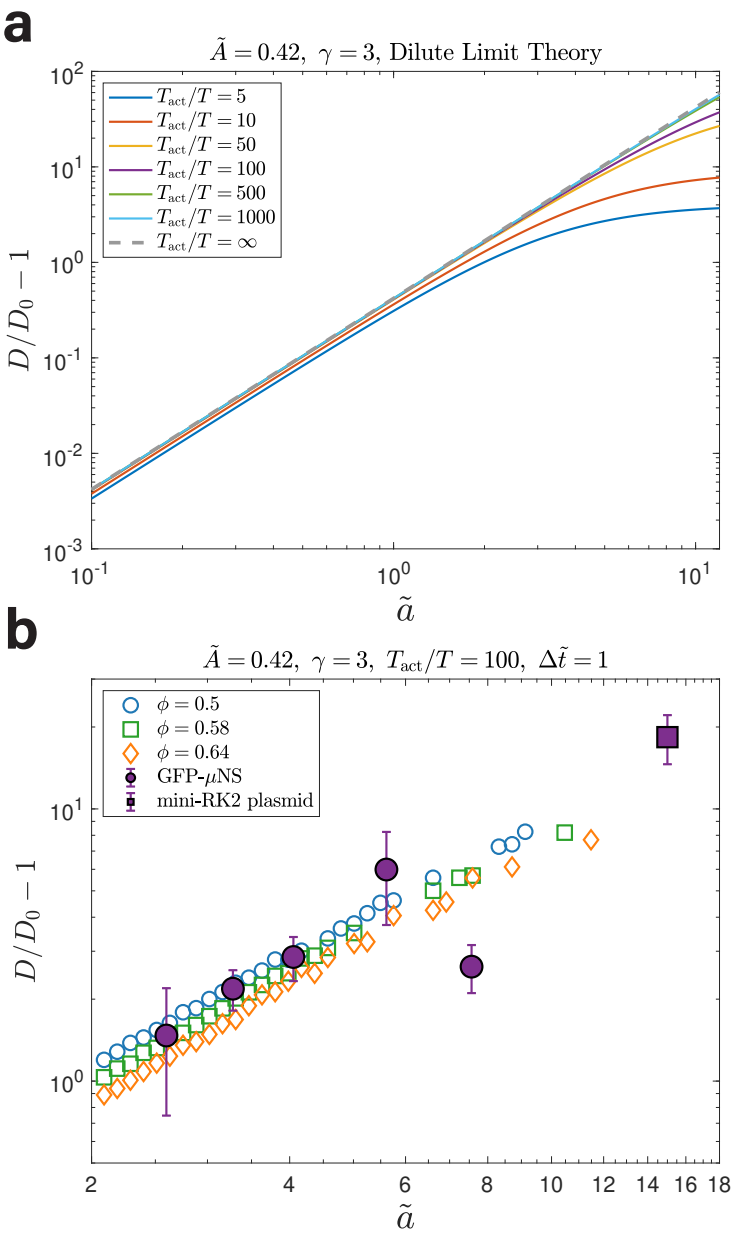

FIG. S14. Effects of the additional active friction coefficient. (a) The diffusion enhancement $D/D_0 - 1$ for different active temperatures T_{act} from Eq. (1) in the dilute limit. When the active temperature is high, the effects of the active friction are negligible. (b) Comparison between simulations using Eq. (1) with $T_{act} = 100T$ and experiments. The relative enhancements of diffusion constants from the experimental data match the simulation results well. In both panels, $\tilde{A} = 0.42$ and $\gamma = 3$. In (b), the results are binned over particles with a bin interval of 0.02 in the $\log_{10}$ scale and $N = 1000$.